Arbitrarily High Order BGK-Shakhov Method for the Simulation of Micro-Channel Flows

D. M. Bond[1]**, V. Wheatley**[1]**, M. N. Macrossan**[1] **and M. Goldsworthy**[2]

[1]School of Mechanical and Mining Engineering, University of Queensland, St Lucia 4072, Australia
[2]CSIRO Energy Technology, Newcastle 2304, Australia

Abstract

A new arbitrarily high order method for the solution of the model Boltzmann equation for micro-channel flows in the transitional regime is presented. The Bhattnagar-Gross-Krook approximation of the Boltzmann collision integral is implemented, with Shakhov's modification, and the resulting system of equations solved by a discrete ordinate method. The method approximates velocity space using a truncated Hermite polynomial expansion of arbitrary order and performs the associated integration by Gauss-Hermite quadrature. This approach conserves mass, momentum and energy during relaxation of the discretised velocity space towards equilibrium. Physical space is discretised by discontinuous Legendre polynomial expansions with both the spatial representation and conservative flux calculation being of arbitrary order. Owing to the high order spatial representation of the discretised velocity space the BGK-Shakhov relaxation process is carried out in a 'continuous in space' manner. New high order boundary conditions of the inviscid slip wall and no-slip wall are implemented. A new fully diffuse reflection boundary condition, built on the high order spatial information available in the method, is also proposed. Results are presented for low speed planar Couette flow and non-linear channel flow.

Introduction

The Boltzmann equation, which describes the evolution of the velocity distribution of a dilute monatomic gas through binary elastic collisions, allows the simulation of flows through the transitional regime, and beyond, where the Navier-Stokes equations are not valid. Methods that allow the efficient solution of the Boltzmann equation are therefore highly sought after.

The Boltzmann equation,

$$\frac{\partial f}{\partial t} + \vec{\xi} \cdot \frac{\partial f}{\partial \vec{x}} = \Omega(f) \approx \nu\left(f^{\text{target}} - f\right), \qquad (1)$$

describes the gas flow in terms of the velocity distribution function, $f = f\left(\vec{x}, \vec{\xi}, t\right)$, which is a function of position, $\vec{x}$, microscopic absolute velocity, $\vec{\xi}$, and time, t. The non-linear integral collision term, $\Omega(f)$, is numerically expensive to calculate and can be replaced with the much simpler Bhattnagar-Gross-Krook (BGK) model [1], as shown, which relaxes f towards a known target distribution, f^{target}, with relaxation frequency ν. To circumvent the fixed Prandtl number (Pr = 1) limitation of the BGK model, the Shakhov target distribution may be used [2]. The Shakhov distribution includes the heat flux vector, $\vec{q}$, as an input which is itself a moment of f.

To solve Eq. (1) numerically, the discrete ordinate method (DOM) [3] may be used, whereby the continuous velocity distribution function is replaced by multiple discrete distributions, $f_i(\vec{x}, t)$, each with a corresponding constant advection velocity, $\vec{\xi}_i$. To enforce conservation of mass, momentum and energy, in an efficient manner, the continuous distribution function, $f\left(\vec{x}, \vec{\xi}, t\right)$, may be approximated as a truncated Hermite polynomial [4]. The discrete distributions of the DOM then correspond to the prescribed abscissa of the Gauss-Hermite quadrature rule selected to allow exact integration of the Hermite polynomial.

The linear advection component of Eq. (1) may be implemented using any number of techniques including finite difference, volume, and element approaches. Recently, a scheme that uses discontinuous truncated Legendre polynomials to represent high order spatial variations has been proposed [5]. This method uses the high order information within each finite volume cell to perform linear advection and so presents a uniformly high order scheme that is well suited to the DOM approach.

In this paper we give a brief description of the numerical method before outlining the high order boundary conditions that have been implemented and their related issues. Results for channel flows are then displayed with an investigation into the order of convergence of the method and the effect of rarefaction on heat flux into the wall for planar Couette flow.

The Numerical Method

In this section a brief overview of the numerical method will be presented, for a more complete description refer to Bond *et al.* [6]. The Boltzmann equation, given in Eq. (1), can be written in discrete form while maintaining exact recovery of all moments of the velocity distribution function up to some arbitrary order, by mapping $f\left(\vec{x}, \vec{\xi}, t\right)$ onto a Hermite subspace according to the method of Shan *et al.*[4]. The continuous form of the equations is then reduced to a set of discrete distributions, one for each of the velocity abscissa, $\vec{\xi}_k$, required by the Gauss-Hermite quadrature rule. By replacing the collision operator, Ω, with the BGK-Shakhov approximation and a reduction of the spatial dimension, by the method of Chu [7], the Boltzmann equation can be written according to Eqs. (2). The g and h terms relate to the translational and thermal energy components, respectively, of the original distribution function, f, while the g_k^S and h_k^S denote the use of the Shakhov model as the target distribution.

$$\frac{\partial g_k}{\partial t} + \vec{\xi} \frac{\partial g_k}{\partial \vec{x}} = \nu\left(g_k^S - g_k\right) \qquad \frac{\partial h_k}{\partial t} + \vec{\xi} \frac{\partial h_k}{\partial \vec{x}} = \nu\left(h_k^S - h_k\right) \quad (2)$$

From this point on it should be noted that all vector quantities refer to only two spatial variables i.e. $\vec{\xi} = [u, v]$.

Nondimensionalisation

We define a characteristic length, L, and speed, C_∞, and the characteristic time, t_∞, follows accordingly in Eq. (3). A characteristic density, ρ_∞, and temperature, T_∞ are also required.

$$C_\infty = \sqrt{RT_\infty} \qquad\qquad t_\infty = \frac{L}{C_\infty} \qquad (3)$$

The non-dimensional variables for absolute molecular velocity, $\vec{\xi}$, mean macroscopic velocity, $\vec{\Xi}$, relaxation frequency, ν, and the stress, $\vec{\tau}$, heat flux, $\vec{q}$, and acceleration, $\vec{a}$, vectors can then be introduced in Eqs. (4).

$$\hat{\vec{x}} = \vec{x}/L \qquad \hat{\vec{\xi}} = \vec{\xi}/C_\infty \qquad \hat{\vec{\Xi}} = \vec{\Xi}/C_\infty$$
$$\hat{t} = t/t_\infty \qquad \hat{\nu} = \nu t_\infty \qquad \hat{\rho} = \rho/\rho_\infty$$
$$\hat{\theta} = T/T_\infty \qquad \hat{\vec{\tau}} = \vec{\tau}/\rho_\infty C_\infty^2 \qquad \hat{\vec{q}} = \vec{q}/\rho_\infty C_\infty^3$$
$$\hat{\vec{a}} = \vec{a}/(L/RT_\infty) \qquad \hat{g} = g/\left(\rho_\infty/C_\infty^2\right) \qquad \hat{h} = h/\rho_\infty$$
$$\text{Kn} = \lambda/L \qquad\qquad (4)$$

The Knudsen number, Kn, indicates the degree of translational non-equilibrium in the flow.

All quantities from this point on, unless otherwise specified, will be in non-dimensional form and the carats will be omitted. The Shakhov distributions for g_k and h_k, used as the target distribution in Eqs. (2), can then be given in non-dimensional form according to Eqs. (5-6).

$$g_k^S = g_k^M \left[1 - \frac{(\text{Pr} - 1)(\vec{q} \cdot \vec{c}_k)(\vec{c}_k \cdot \vec{c}_k - 4\theta)}{5\theta^3 \rho} \right] \qquad (5)$$

$$h_k^S = g_k^M \theta \left[1 - \frac{(\text{Pr} - 1)(\vec{q} \cdot \vec{c}_k)(\vec{c}_k \cdot \vec{c}_k - 2\theta)}{5\theta^3 \rho} \right] \qquad (6)$$

$$g_k^M = \frac{\rho}{2\pi\theta} \exp\left(-\frac{\vec{c}_k \cdot \vec{c}_k}{2\theta} \right) \qquad (7)$$

The peculiar velocity, $\vec{c}_k$, is given by $\vec{c}_k = \vec{\xi}_k - \vec{\Xi}_k$ and the non-dimensional collision frequency, Eq. (8), which determines the rate of relaxation can also be defined. The variable ω is the exponent of the power law viscosity although other viscosity laws can be used.

$$\nu = \frac{\rho}{\text{Kn}} \sqrt{\frac{\pi}{2}} \theta^{1-\omega} \qquad (8)$$

Spatial Representation

The solution of the set of discrete equations given in Eqs. (2), by the process of linear advection and relaxation, allows for the implementation of an explicit linear advection solver. The Conservative Flux Approximation (CFA) method of Latorre et al.[5] solves the linear advection equation in multi-dimensional situations in a high order manner. The CFA method representats each discrete distribution, g_k and h_k, as a truncated expansion in Legendre polynomials, of order N_l, in space that is discontinuous across cell interfaces. This can be expressed for the k-th distribution in cell (i,j) according to Eqs. (9-10).

$$g_{i,j,k}(\vec{x}) = \sum_{m=1}^{N_l} \sum_{n=1}^{N_l} a_{i,j,k}^{(m,n)} \mathcal{L}_m(x) \mathcal{L}_n(y) \approx g_{i,j,k}^{\text{exact}}(\vec{x}) \qquad (9)$$

$$a_{i,j,k}^{(m,n)} = \frac{(2m-1)(2n-1)}{4} \iint_{-1}^{1} g_{i,j,k}^{\text{exact}}(\vec{x}) \mathcal{L}_m(x) \mathcal{L}_n(y) \, dx dy \qquad (10)$$

The polynomial representation given by Eq. (9) is encoded in the coefficient matrix $\mathbf{a}$, of which $a^{(m,n)}$ is the coefficient corre-

sponding to the product of the mth and n^{th} order Legendre polynomials. The exact expression for the advection of the polynomial representaton is given by Eq. (11) and can be seen, for a 1D example with positive advection velocity, in the first two panels of Fig. 1.

$$g_k(\vec{x}, t + \Delta t) = g_k\left(\vec{x} - \vec{\xi}_k \Delta t, t\right) \qquad (11)$$
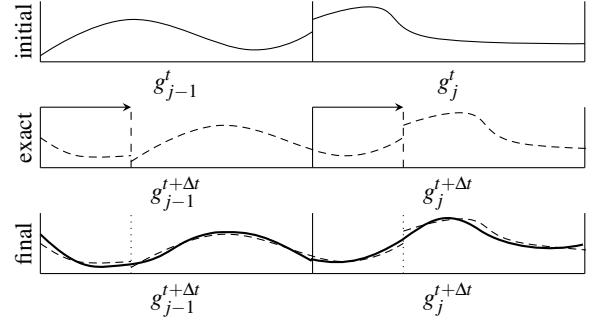

Figure 1: Initial distribution, exact advected solution and final approximate solution (–) after remapping the exact solution (- -) onto the local polynomial basis. This figure is illustrative only.

By mapping this exact solution, Eq. (11), back onto the truncated Legendre basis in each cell, according to Eq. (10), we obtain new expansion coefficients in that cell. These new coefficients describe a high order approximation to the solution of the exact advection equation at the next time step, seen in the third panel of Fig. 1. In the cell local reference frame, the solution to be mapped onto the Legendre basis can be expressed in terms of the neighbouring polynomial expansions depending on the advection velocity, time step, and local cell size. Note that this process does not require smoothly varying cell spacing. For full details of the procedure in one and two spatial dimensions the reader is referred to the paper by Latorre et al. [5].

Boundary Conditions

The new boundary schemes developed for this method have been designed to maintain the arbitrarily high order nature of the method and are outlined in the following subsections.

Inviscid Slip & No-Slip Wall

The inviscid wall boundary condition requires the reflection of all incoming velocities with no loss in momentum. This is accomplished with ghost cells that mirror the high order interior cell representations of g_k and h_k in both physical and velocity space about the domain boundary. Conservation is enforced continuously in space and time as the overall density distribution is mirrored as shown in the first panel of Fig. 2. To introduce a no-slip boundary condition requires the same mirroring operations as for the inviscid case with the addition of an extra reflection of the velocity space about the plane perpendicular to the interface. This enforces the complete transfer of tangential momentum from the gas to the wall at the interface. Both of these approaches are shown schematically in Fig. 2.

Diffuse Reflection

The diffuse reflection boundary condition requires that all flux out of the wall is in an equilibrium state defined by the temperature and velocity of the wall, Eq. (7), while preserving instantaneous conservation of mass continuously along the boundary. This is achieved with the following procedure. Firstly, the interior discrete distributions, $g_k(\vec{x})$, are reflected about the wall
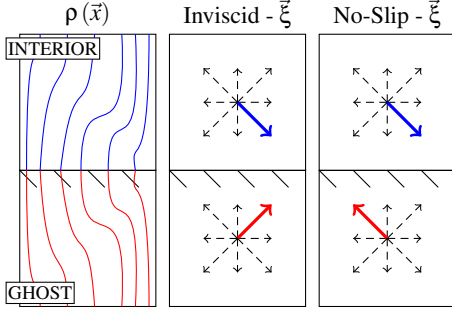
Figure 2: Manipulation of the distribution in physical and velocity space. Inviscid and no-slip wall boundary conditions.

and loaded into the ghost cell. The total mass flux out of the ghost cell over the next time step, $m^{\mathrm{non-eq}}$, is then calculated based on the mirrored ghost distributions. The distribution of density, within the ghost cell, is also calculated from a summation of all the discrete distributions giving a density map $\rho(\vec{x})$. Each g_k and h_k in the ghost cell is then re-calculated according to the Maxwellian distribution defined by the wall temperature and velocity and the spatial density map. A new measure of the flux out of the ghost cell, m^{eq}, is then calculated based on these updated, equilibrium, discrete distributions. By comparing the total mass fluxes from the ghost cell into the flow domain, $\alpha = m^{\mathrm{non-eq}}/m^{\mathrm{eq}}$, calculated from the non-equilibrium and equilibrium distributions, the value of all g_k and h_k are uniformly scaled, by α, to enforce mass conservation.

This procedure uses the high-order information available in the cell to enforce instantaneous mass conservation at any point on the boundary rather than time-averaged conservation, which is typically used in finite-volume methods.

Results

The results in this section are all computed using fourth order polynomials and so should theoretically achieve fourth-order convergence in space. The convergence of the method with no-slip and diffuse boundaries was tested using the Landau and Lifshitz [8] test case of a steepening wave, which forms a shock at t_{shock}, with wall boundaries in y. The domain with periodic conditions in x, on $-1 \le x \le 1$, was initialised with conditions given below, where the sound speed is given by a_0 and ratio of specific heats by γ. The results can be seen in Fig. 3 with convergence in the L_2 and L_∞ norms of density displayed. These results will be discussed in the next section.

$$\rho(x,0) = \rho_0 \left(1 + \frac{(\gamma-1)u_x}{2a_0}\right)^{\frac{2}{\gamma-1}},$$

$$p(x,0) = p_0 \left(1 + \frac{(\gamma-1)u_x}{2a_0}\right)^{\frac{2\gamma}{\gamma-1}},$$

$$u_x(x,0) = u_0 \sin\pi x, u_y = u_z = 0$$

The accuracy of the diffuse boundary condition was verified using the planar Couette flow with results shown to converge to the analytical solution of Sofonea et al. [9] in Fig. 4, the spatial convergence of the $\gamma = 5/3$ test case is also shown.

The heat flux into the wall in the planar Couette flow for a range of Knudsen numbers, through the transitional regime, was also computed and can be seen in Fig. 5.
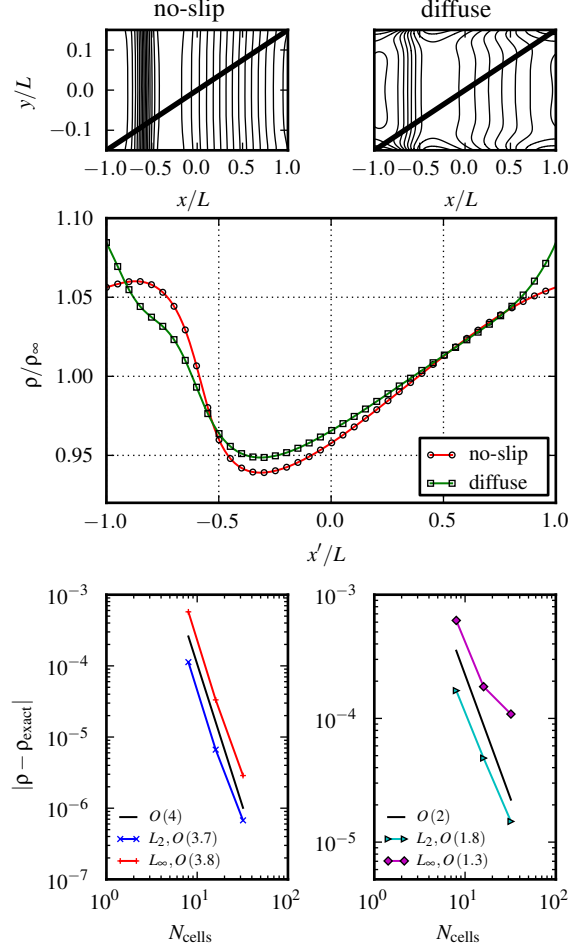
Discussion

Figure 3: Density distribution over the domain, density distribution along the line marked in the contour plot and spatial convergence for the Landau and Lifshitz test case. $[\gamma = 5/3, \mathrm{Pr} = 0.7, \mathrm{Kn} = 0.003, N_l = 4, t = 0.8t_{\mathrm{shock}}]$
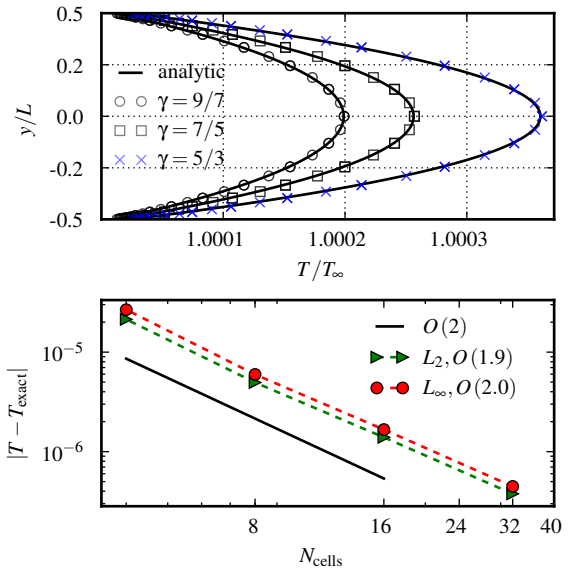

Figure 4: Planar Couette profiles for a range of specific heat ratios. Convergence for $\gamma = 5/3$. $[\mathrm{Pr} = 0.7, N_{\mathrm{cells}} = 20, \mathrm{Kn} = 0.01, N_l = 4, U_{\mathrm{slip}} = 0.1]$
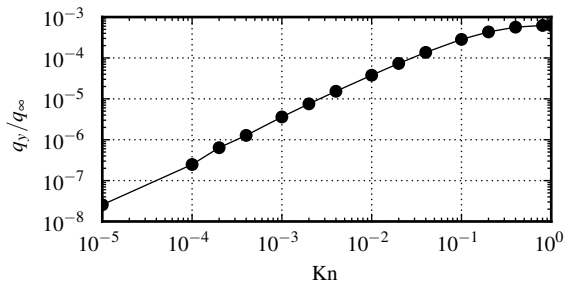
Figure 5: Calculated heat flux into a fully diffuse wall for Planar Couette flow. (Symbols indicate computed values) $\left[\gamma = 5/3, \mathrm{Pr} = 0.7, N_{\mathrm{cells}} = 32, N_l = 4, U_{\mathrm{slip}} = 0.1\right]$

The results shown in Fig. 3 clearly demonstrate that our high-order, no-slip boundary scheme results in convergence at the full theoretical order (4th order). This validates the approach of reflection in physical and velocity space. While the planar Couette flow simulation with diffuse wall shows close agreement with the analytical solution in Fig. 4, the convergence results for the Couette and Landau-Lifshitz test cases show that the method is not achieving the theoretical order of convergence. The reason for this discrepancy has been suggested by Alekseenko et al.[10] for the Discontinuous-Galerkin (DG) method. The problem can be traced to the introduction of a discontinuity into each discrete distribution by the ghost cells representing flow from the wall into the fluid domain. For the diffuse wall, this is due to the wall distribution being defined according to the state of the wall rather than the state of the fluid. This discontinuity is introduced into the flow domain at each time-step, shown in Fig. 6, and eliminates the smooth nature of the distribution required for high-order convergence. An interesting feature of Fig. 6 is the large effect that relaxation has on the final form of the discrete distribution.
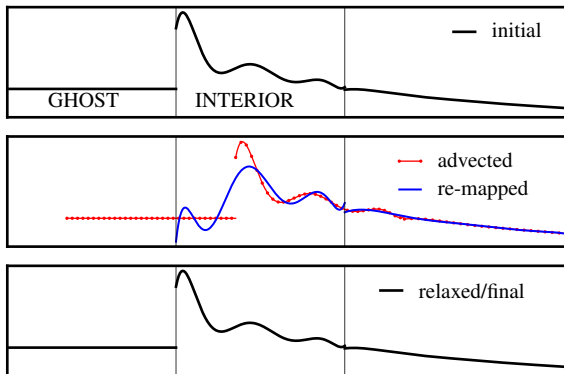

Figure 6: Normalised discrete distribution near a diffuse wall. Note: These results show actual simulation data.

While this method is able to accurately simulate gaseous flows this reduction in order of convergence has the overall effect of removing the efficiency incentive for using this high order method with the diffuse wall boundary scheme. The method still, however, retains a conceptually superior model of relaxation and transport and may prove to have higher accuracy with the same order of convergence (2nd order) when compared to traditional finite-volume methods.

The heat flux into the diffuse wall for varying Knudsen numbers displays a trend of increasing heat flux until the mean free path is equal to the channel width with orders of magnitude increase in heat transfer from the continuum to rarefied regime. This demonstrates the capability of the numerical method to make predictions across the entire transitional regime. While these results require further validation they provide an indication of how using micro-channels with significant rarefaction can increase heat transfer in real world applications.

Conclusions

A new method of arbitrarily high-order discretisation of the BGK-Shakhov equation in physical and velocity space has been presented. High order boundary conditions for the inviscid slip wall and no-slip wall have been implemented and shown to achieve high order convergence using the Landau-Lifshitz test case with wall boundaries. A fully diffuse reflection boundary condition has also been implemented with inherent limitations exposed. Results for planar Couette flow, with the diffuse wall, showing the accuracy of the scheme and the variation of heat flux with Knudsen number have also been presented.

Acknowledgements

References

[1] P. L. Bhatnagar, E. P. Gross, and M. Krook. A Model for Collision Processes in Gases. I. Small Amplitude Processes in Charged and Neutral One-Component Systems. *Phys. Rev.*, 94:511–525, May 1954.

[2] E. M. Shakhov. Generalization of the Krook kinetic relaxation equation. *Fluid Dynamics*, 3:95–96, 1968. 10.1007/BF01029546.

[3] J. Y. Yang, J. C. Huang, and L. Tsuei. Numerical Solutions of the Nonlinear Model Boltzmann Equations. *Proceedings: Mathematical and Physical Sciences*, 448(1932):pp. 55–80, 1995.

[4] Xiaowen Shan, Xue-Feng Yuan, and Hudong Chen. Kinetic theory representation of hydrodynamics: a way beyond the Navier-Stokes equation. *Journal of Fluid Mechanics*, 550:413–441, 2006.

[5] B. Latorre, P. Garcia-Navarro, J. Murillo, and J. Burguete. Accurate and efficient simulation of transport in multi-dimensional flow. *International Journal for Numerical Methods in Fluids*, 65(4):405–431, 2011.

[6] D.M. Bond, M.N. Macrossan, and V.Wheatley. Comparison of discrete BGK-Shakhov system with DSMC. to appear in Rarefied Gas Dynamics: proceedings of the 28th International Symposium on Rarefied Gas Dynamics, Zaragoza, Spain, July 2012.

[7] C. K. Chu. Kinetic-Theoretic Description of the Formation of a Shock Wave. *Physics of Fluids*, 8(1):12–22, 1965.

[8] L.D. Landau and E.M. Lifshitz. *Fluid Mechanics*. Butterworth-Heinemann, 1987.

[9] Victor Sofonea and Robert F. Sekerka. Diffuse-reflection boundary conditions for a thermal lattice Boltzmann model in two dimensions: Evidence of temperature jump and slip velocity in microchannels. *Phys. Rev. E*, 71(6):066709, Jun 2005.

[10] A. Alekseenko, N. Gimelshein, and S. Gimelshein. An application of Discontinuous Galerkin space and velocity discretisations to the solution of a model kinetic equation. *International Journal of Computational Fluid Dynamics*, 26(3):145–161, 2012.